Ferroresonance case study in a distribution network and the potential impact of DERs and CVR/VVO

Gaurish S. Gokhale, Bruce A. Mork, John O. Donnell Jr, Steven R. Brehmer

***Abstract*—Ferroresonance in single-phase, line-to-line connected transformers in an ungrounded distribution system with delta-connected capacitors is possible but has not been reported in recent literature. In this paper, a high voltage event that actually occurred in an ungrounded distribution network with multiple distribution transformers has been simulated for lessons learned. The hypothesis was that ferroresonance was the cause of the overvoltage event in the network after a single-phase event led to sustained voltages of 1.45 p.u. Simulations were performed and ferroresonance was found to be the possible cause for the overvoltages. One of the prevention solutions found to avoid the overvoltages was to balance the loads on the three phases.**

The increased deployment of CVR/VVO strategies leads to circuit configurations similar to that studied in this paper and could lead to an increased likelihood of ferroresonance, if it is not fully understood and addressed. The impact of additional single-phase solar inverters on the low voltage side of the transformers was also studied. The results obtained show that the effective loading of the transformers, which is the difference in the actual load connected and the output from the DER, proved to be the deciding factor for initiation of ferroresonance in such networks.

Keywords—distribution transformers, EMT simulations, ferroresonance, shunt capacitor banks, single-phase inverters

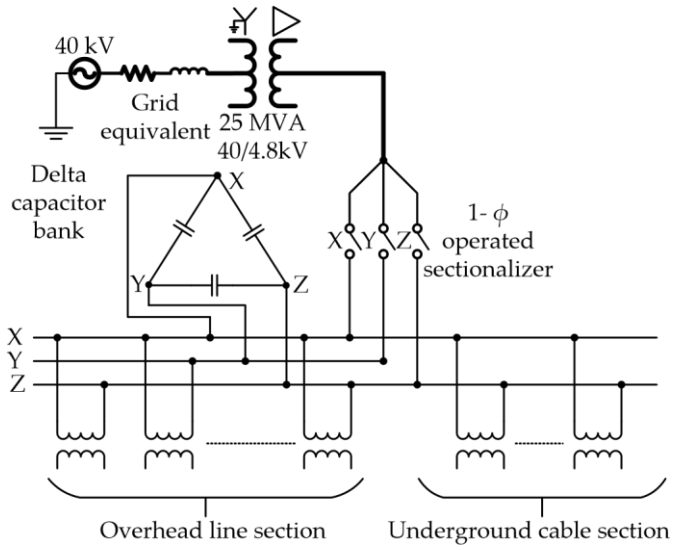

Figure 1. Three line diagram of the system under study

I. Introduction

THE use of Conservation Voltage Reduction (CVR)/ Volt-VAR Optimization (VVO) strategies by utilities modify the circuit parameters by addition of compensating devices in distribution network. Additionally, distribution networks may have phase imbalances, lightly loaded transformers and singlephase operated sectionalizing devices. Further, the increase in renewable generation typically in the form of residential solar inverters create a bidirectional power flow in the network. All these factors combine to create the operating scenarios which are different from the balanced, grounded and radial distribution networks.

An actual overvoltage event occurred with the type of circuit configuration described above and shown in Figure 1, with the deployment of shunt compensation. Although the likelihood of such an event occurring in a distribution circuit is low with the existing configuration and has not been reported in the literature, the increasing use of CVR/VVO deployment along with the increase in Distributed Energy Resources (DER) penetration in the distribution system may lead to a higher likelihood of the occurrence of such events in distribution systems in the future.

CVR/VVO strategies have the promise to be a cost-effective measure for energy savings and peak demand reduction. As the load in the system varies with several factors such as temperature, season and time of day, the control of shunt capacitor banks for CVR/VVO is based on one or more of these [1]. Ferroresonance is one of the power quality issues that needs consideration with the use of shunt capacitor banks, especially in a single-phase switched distribution network consisting of multiple single-phase transformers and an ungrounded shunt capacitor bank [2].

According to IEEE 1547-2018 [3], inverter-based generation can supply both active and reactive power. This presents an opportunity to control the distribution feeder voltages in a decentralized manner, which would have been otherwise centrally controlled with the traditional CVR/VVO equipment [4]. However, the addition of inverter-based generation connected to the utility distribution system can cause issues such as overvoltage and ferroresonance [5].

Ferroresonance is defined in [6] as the overvoltage associated with the excitation of one or more saturable inductors through a series capacitance. The elements required for ferroresonance to occur are a nonlinear inductance, a capacitance, low losses, and a source [7], [8]. The low losses are associated with light-loaded transformers, which fail to provide sufficient damping in the system. In addition, a switching event is required to initiate ferroresonance in the network. The saturable inductor in power systems is usually the

This work was supported in part by DTE Energy, USA.

G. S. Gokhale and B. A. Mork are with Michigan Technological University, Houghton, MI 49931, USA (e-mail of corresponding author: ggokhale@mtu.edu).

J. O. Donnell Jr. and S. R. Brehmer are with the DTE Energy, Detroit, MI, USA.

Paper submitted to the International Conference on Power Systems Transients (IPST2023) in Thessaloniki, Greece, June 12-15, 2023.

magnetizing branch of either power transformers or voltage transformers. Network configurations vulnerable to ferroresonance have been identified in [9], some of which are power transformers terminated double-circuit or series compensated transmission lines, voltage transformers (VTs) in ungrounded neutral configuration, line VTs with circuit breaker grading capacitors.

The literature published on ferroresonance in distribution circuits primarily focuses on three-phase distribution transformers. Ferroresonance can also occur in phase-to-phase connected single-phase distribution transformers [10], [11] or phase-to-ground connected single-phase distribution transformers on a three-phase distribution circuit [12]. Underground cable is one of the contributors to the capacitive nature of the circuit [13], [14]. Shunt capacitor bank used for reactive power compensation is another source of the capacitive nature [15], [16].

Some ways to mitigate ferroresonance in distribution networks have been listed below from the available literature.

- Elimination of asymmetrical switching [14], [17], [18]
- Coordinated operation of cable and transformer [14]
- Maintain transformer loading during energization [14], [17], [18]
- Modifications in circuit configuration [14], [17]
- Voltage controlled resistor in neutral [17], [19], [20]

In the distribution network under study, all the elements for the occurrence of ferroresonance were present: the nonlinear inductance in the form of twelve single-phase distribution transformers, the capacitance of the shunt capacitor bank and a section of underground cable, light-loaded hours of the day, and the occurrence of a single-phase event that had caused one phase to be disconnected from the network, while the other two phases were energized. All these factors, along with a recorded voltage of 1.45 p.u., led to the hypothesis of ferroresonance event in the network.

With the increasing penetration of single-phase, grid-connected, solar inverters connected on the secondary of distribution transformers, the impact they have on conventional power system transients such as ferroresonance should be studied. There has been some work done with the aspects of interconnection transformer configuration impact on ferroresonance [21] but it is applicable to the larger three-phase solar farms. The occurrence of ferroresonance on the low voltage side of a three-phase transformer has been discussed in [22].

However, there is no literature which discusses the impact of the single-phase solar inverters on the initiation of ferroresonance. To observe any such behavior in the distribution network under consideration, an extended study to analyse the impact of single-phase solar inverters connected on the low-voltage side of the distribution transformer was performed.

The system under study will be presented in Section II along with the sequence of events. To evaluate the hypothesis of ferroresonance, electromagnetic transients (EMT) simulations were performed with the knowledge of the network parameters and suitable assumptions of the unknown parameters, which will be discussed in Section III. Along with the actual network modeling details, the details of single-phase inverter modeling will also be discussed separately in Section IV.

Section V presents the results of the simulations carried out while Section VI focuses on the analysis of the results obtained by the addition of DER in the distribution network and its impact on ferroresonance. Prevention and mitigation strategies to avoid ferroresonance in networks similar to the one being studied are presented in Section VII. One of the surprising prevention strategies highlights the importance of phase-balancing, which could have avoided this overvoltage event. This prevention strategy has not been reported in the literature. This makes the outcomes of this paper effective against similar existing or upcoming configurations in distribution networks.

II. System description and events

A. System description

The distribution network shown in Figure 1 is an ungrounded delta circuit at a voltage level of 4.8 kV. This network is downstream of a 40/4.8 kV, grounded-wye to delta transformer. Although it is common to have grounded distribution networks, the circuit under consideration is an older circuit that is ungrounded and delta-connected.

A single-phase sectionalizing device is connected downstream of the 40/4.8 kV transformer. This portion of the circuit consists of twelve, single-phase, 4.8/0.24 kV, line-to-line connected distribution transformers. The transformers have varying saturation curves.

Of the twelve transformers, six transformers are connected through overhead lines whereas the other six are connected through underground cables. The phase nomenclature used in this circuit is X, Y and Z for the three phases. All the six transformers connected through the underground cable are only connected between phases X-Z, thus only these two cables are connected. There is no cable run for the Y phase. The circuit was highly unbalanced, since 11 of the transformers are connected on the X-Z phases while only 1 transformer was connected on the X-Y phase. There were no transformers on the Y-Z phases.

The overhead section of the circuit has a 600 kVAR, 4.8kV, delta-connected, shunt capacitor bank. This capacitor bank is controlled based on the time-of-day, irrespective of the voltage at the point of connection.

Advanced metering infrastructure (AMI) devices are connected on the low voltage side of the distribution transformers. These devices can record the voltage magnitudes in intervals of 15 minutes.

From the description of the distribution network, a few observations can be made, which differentiate this network from the others presented in the literature for ferroresonance studies.

- The circuit is an ungrounded delta with shunt capacitor banks connected in a delta configuration as well.
- There are multiple transformer samples with varying saturation levels, which were tested and modeled based on the test reports. Sensitivity analysis was carried out to find the combinations vulnerable to overvoltages.
- The load on the three phases is not balanced, so a single-phase simplified circuit cannot be modeled for analysis.

.

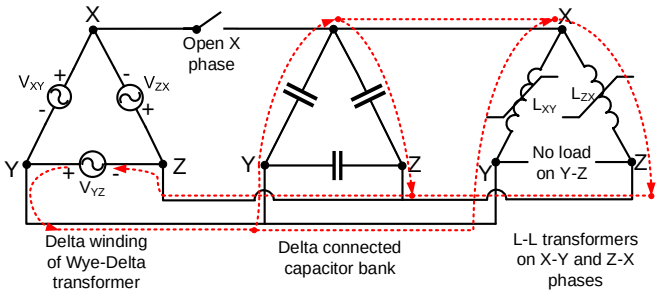

Figure 2. Simplified circuit of the system with open circuit on X phase

- The circuit consists of a combination of overhead lines and underground cables, which have varying levels of capacitances and inductances.
- It is known that the transformers were lightly loaded. The loads at certain points were known but not throughout the event. Sensitivity analysis was performed, and it was found that overvoltage did not exist for load more than 20% of the transformer rating.
- The line-to-line voltage magnitudes were recorded but the waveshapes could not be recorded as this functionality is unavailable in the installed AMI meters. As this is an active circuit with customers connected, recreation of the scenario with waveshape recorders is not possible.

The factors listed above make it difficult to match the simulation results exactly with the field recordings. The goal of the simulation of this system was to find if such a configuration is vulnerable to ferroresonance and to find prevention and mitigation solutions to avoid such an event.

B. Event description

The shunt capacitor bank was controlled based on the time-of-day. The event under study occurred at the time-of-day when the circuit was lightly loaded, but overlapped with the time when the capacitor bank was connected in the circuit.

The event began with the disconnection of X-phase, possibly due to a branch of a tree touching the overhead distribution line and causing a fault. A voltage of 1.45 p.u. was recorded by the AMI on the X-Y phase distribution transformer and 1.35 p.u. on the Z-X phase. The circuit showing the flow of current with the X-phase disconnected has been shown in Figure 2.

The X-Y transformer was damaged after about 20 minutes, while the voltage on the X-Z phase reduced to about 0.5 p.u. The recordings of the AMI are shown in Figures 3 and 4.

III. EMT MODELING OF SYSTEM COMPONENTS

The system model was developed using the EMTP-ATP software [23], and has been shown in Figure 5. Most of the equipment used in the model has sufficient literature available, so a detailed discussion has not be presented. Details of inverter modeling have been presented in detail in a separate section since not much literature has been presented about the single-phase inverter models in EMTP. The line and cable data used in the circuit are similar to those described in Appendix C of [24].

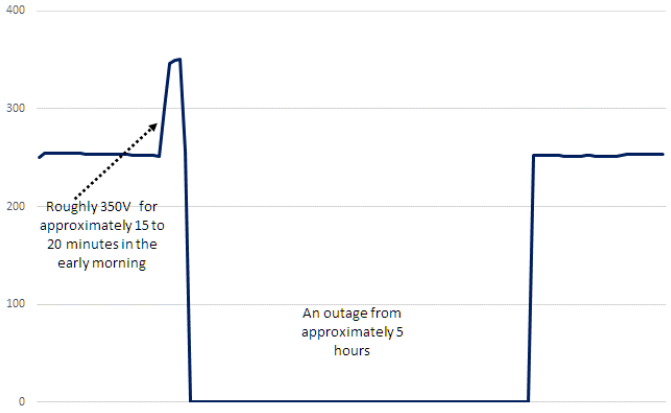

Figure 3. Line-to-line voltage measurements on the X-Y connected transformer

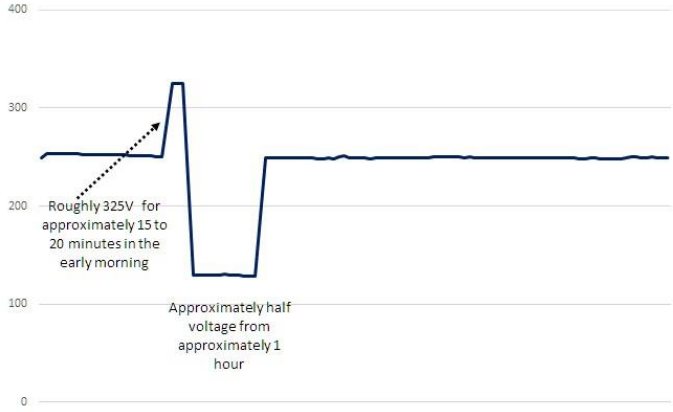

Figure 4. Line-to-line voltage measurements on the X-Z connected transformers

A. Transformer model

The transformers are modeled as shown in Figure 6. The short-circuit and core parameters are referred to the primary side. Core parameters are obtained from lab measurements of true root mean square (RMS) values of voltages (V) and currents (I) at excitation levels up to 1.3 p.u. The core loss resistor is assumed linear and its value is derived from excitation of 1.0 p.u. The magnetizing inductance is modeled by a Type-93 piece-wise nonlinear inductor. The inputs for

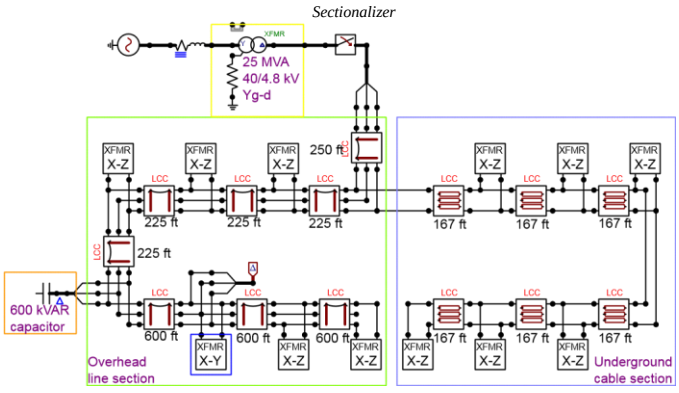

Figure 5. Simulation model of the network in EMTP-ATP

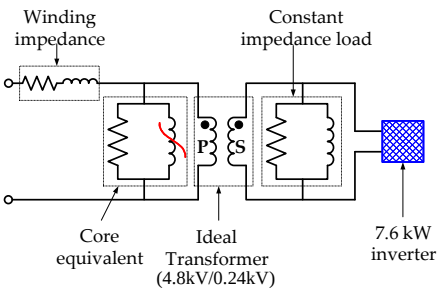

Figure 6. Detailed view of the transformer blocks in Figure 5

the nonlinear inductor are the peak flux linkage, λ *(in Volt-seconds)*, and peak exciting current, *i (in Amperes)*. The RMS V-I measurements are converted to peak λ-*i* values using the supporting routine "SATURA". Note that this method removes the core loss component from the exciting current so that the λ-*i* characteristics represent the magnetizing curve. [25]

The winding parameters of the transformers were modeled based on the values obtained by the load tests performed on similar transformer samples. The transformers were modeled with 100% of the leakage reactance on the 4.8kV side using the T-representation since there is little leakage associated with low voltage windings in single-phase transformers [26]. An ideal single-phase transformer was used to step down the voltage and the load and the inverter were connected to the low voltage side of this transformer, as shown in Figure 6. The transformer parameters were available from the test report performed on the four samples of transformers [27].

B. Shunt capacitor bank

The capacitor bank was in an ungrounded delta configuration. The value of capacitance for the 600 kVAR capacitor bank for 4.8 kV line-to-line voltage can be calculated as shown in Equation 1. In this equation, *Q* is the reactive power rating of the capacitor bank, C is the value of the capacitance of the capacitor bank being calculated, *f* is the system frequency and *V* is the voltage.

$$C = \frac{Q}{2\pi f V^2} \tag{1}$$

C. Load

The loads were modeled as constant impedance loads with a parallel resistance and inductance. The power factor of the load was chosen as 0.9, which is the usual power factor for residential loads.

For a full load of 25 kVA at a power factor of 0.9, the active power is 22.5 kW and the reactive power is 10.89 kVAR. The calculations for full load are shown in Equations 2 and 3. To vary the load connected, the resistance and inductive reactance values have been varied.

In Equations 2 and 3, *R* and *X* are the resistance and the inductive reactance, which are calculated based on the active power, *P* and reactive power, *Q* respectively. *V* is the voltage across the resistance or reactance.

$$R = \frac{V^2}{P} = \frac{240^2}{22.5 * 10^3} = 2.56\ \Omega \tag{2}$$

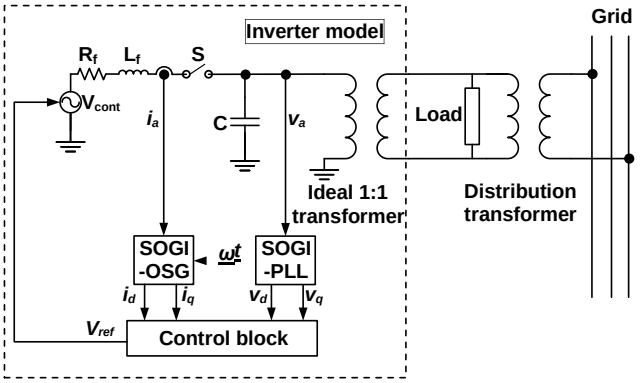

Figure 7. Single-phase VSI connected on LV side of the transformer

$$X = \frac{V^2}{Q} = \frac{240^2}{10.89 * 10^3} = 5.289\ \Omega \tag{3}$$

IV. EMT MODELING OF SINGLE-PHASE INVERTER

Detailed modeling of grid-connected, three-phase inverters has been explained in [28]. However, the major challenge with modeling of single-phase inverters is the absence of orthogonality, which prevents from using the Park transformation in these systems [29]. Park transformation is used to obtain the direct and quadrature axis (*dq*) quantities for inverter controls.

The overall connection diagram of the single-phase voltage source inverter (VSI) has been shown in Figure 7. Second Order Generalized Integrator (SOGI) has been used in this model to first produce the signals in $\alpha\beta$ frame, and then the *dq* frame for inverter controls. The SOGI phase locked loop (SOGI-PLL) has been used to track the phase angle for synchronization.

The control algorithm has been shown in Figure 8. It produces the output voltage based on the inner current control loop and the outer power control loop as discussed in [29]. The average source model described in [30] was used to demonstrate the output of the inverter.

To overcome the absence of an ungrounded controlled source in the software, a grounded source followed by an ideal transformer with a 1:1 turns ratio was used, similar to [31]. The voltages for controls were measured at the capacitance connected on the grid side of the switch whereas the currents were measured at the output of the inverters, just after the R-L filter. The switch S is initially open as the PLL requires a few cycles to track the phase angle.

$$L_f = \frac{V_{dc}}{8 * I_{ripple} * f_{sw}} \tag{4}$$

The inverter specifications are taken from one of the common manufacturer's specification sheet [32]. The filter parameters were calculated as shown in [33]. The calculation for filter inductance, L_f has been shown in Equation 4, which is calculated from the DC bus voltage of the inverter, V_{DC}; the permissible ripple current value, I_{ripple} and the switching frequency, f_{sw}. The inverter specifications and filter calculated values have been mentioned in Table I.

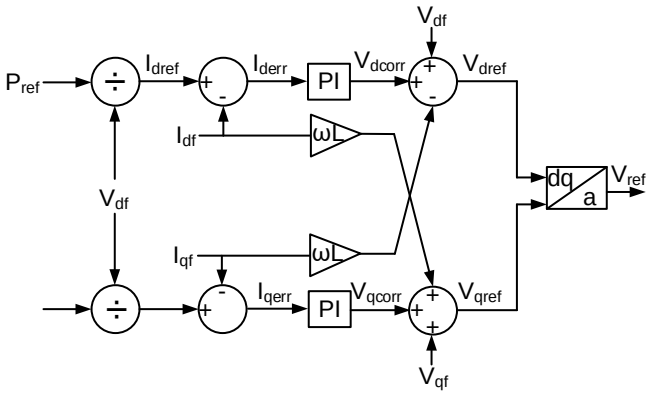

Figure 8. Inverter control algorithm implemented in the model

Table I
INVERTER SPECIFICATIONS AND FILTER VALUES

Parameter	Rating	Parameter	Rating
Power	7.6 kW	Filter inductance	2.1 mH
L-L voltage	240 V	Quality factor	30
DC voltage	380 V	Filter resistance	0.0264 Ω
Switching frequency	5 kHz	Capacitance	35 μF

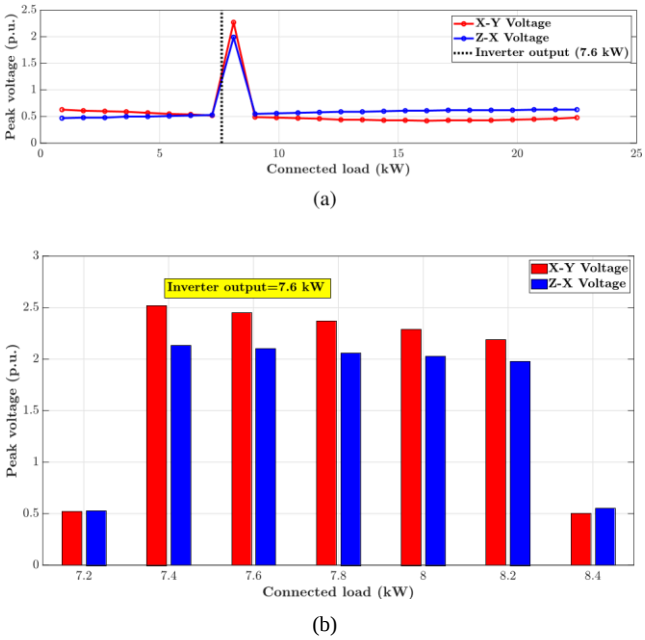

Figure 10. Impact of inverter on the connected load causing overvoltages (a)Variation of load from 0.9 kW to 22.5 kW in increments of 1 kW (b)Variation of load from 7.2 kW to 8.4 kW in increments of 0.2 kW

V. RESULTS AND DISCUSSION

A. Ferroresonance in the actual circuit

As described earlier in the paper, the number of unknowns in the system created an infinite number of combinations based on the loads connected on the different transformers and the transformer samples present in the system. Also, ferroresonance being a nonlinear phenomena, a linear extrapolation for assumptions cannot be performed. Thus, the aim was to check the possibility of occurrence of ferroresonance in the network with the known parameters and the assumptions of the unknown.

The voltage waveforms shown in Figure 9 were obtained by opening the X-phase of the 1-Φ sectionalizer shown in Figure 1. From Figure 9, it is seen that the peak voltage on the X-Y phase was about 2.08 p.u. while on the Z-X phase, it was 1.88 p.u.

Ferroresonance is a nonlinear resonance which results in voltage waveforms being distorted. The voltage waveforms in Figure 9 are distorted and not in the linear region of operation. This was confirmed by examining the operating point of the λ-i curves of the transformers involved.

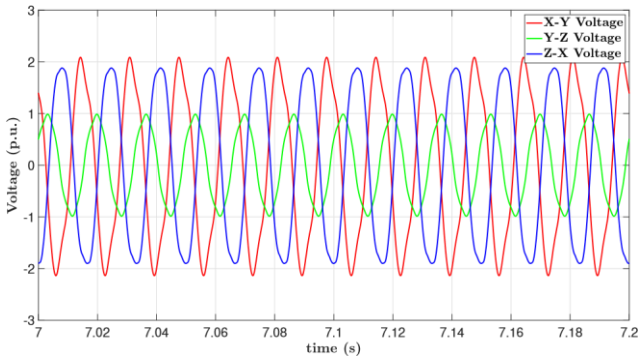

Figure 9. Line-to-line voltages measured at the X-Y connected transformer terminal after opening X-phase in the system model

In addition, to verify that the overvoltage had indeed been caused due to ferroresonance, one of these parameters was varied at a time:

- Using transformer cores with higher knee-point in the distribution network
- Gradually increasing the load from no load to full load rating of the transformers
- Simulating the circuit without the shunt capacitor bank
- Switching out all the three-phases together (i.e. disconnecting all phases instead of just the X-phase)

The items listed above are the elements required for ferroresonance to occur in the circuit [7]. When any of these four changes was made, then the overvoltages and distorted waveforms were not observed indicating ferroresonance was the cause.

B. Ferroresonance with addition of DER

To study the effect of addition of DER in the distribution network on ferroresonance, one single-phase inverter was added on each of the twelve line-to-line connected, single-phase transformers in the EMT model shown in Figure 5. The output of these inverters in an actual system would depend on the weather conditions, but for simplicity in simulations the inverters are set to generate a maximum power of 7.6 kW (only active power). [32] It is useful to know that the inverter output reduces the net loading on transformers and hence the damping effects which suppress ferroresonance.

The X-phase of the sectionalizer was then opened to recreate the open-phase event. However, unlike the case discussed for ferroresonance in the actual circuit, no ferroresonance was observed in this case when the transformers were lightly loaded,

Table II
ACTUAL LOADING AND EFFECTIVE LOADING OF TRANSFORMER

S_{LOAD}	P_{LOAD}	$P_{DIFF} = P_{LOAD} - P_{INV}$	P_{ACTUAL}	P_{EFF}
8 kVA	7.2 kW	-0.4 kW	28.8 %	-1.6 %
8.22 kVA	7.4 kW	-0.2 kW	29.6 %	-0.8 %
8.44 kVA	7.6 kW	0 kW	30.4 %	0 %
8.66 kVA	7.8 kW	0.2 kW	31.2 %	0.8 %
8.88 kVA	8 kW	0.4 kW	32 %	1.6 %
9.11 kVA	8.2 kW	0.6 kW	32.8 %	2.4 %
9.33 kVA	8.4 kW	0.8 kW	33.6 %	3.2 %

which can be seen from Figure 10a. The circuit analysis and the explanation for this behavior has been discussed in Section VI.

The loads connected on the transformers were increased from 0.9 kW (4% of transformer rating) to 22.5 kW (100% of transformer rating) in steps of 0.9 kW. Overvoltages were observed closer to the inverter output power rating of 7.6 kW, shown by the dotted line in Figure 10a.

The active power of the load was drawn from the inverter in this case while only the reactive power was drawn from the grid. The step size to vary the loads was then reduced to 0.2 kW closer to the point where the overvoltages were observed in Figure 10a. The results for this test have been presented in Figure 10b. The actual and effective loads connected in Figure 10b has been shown in Table II.

S_{LOAD} is the actual load connected on the transformer secondary in kVA. P_{LOAD} is the actual load connected in the system and P_{DIFF} is the difference of the load active power (P_{LOAD}) and the power supplied by the inverter, P_{INV} (7.6kW). P_{ACTUAL} and P_{DIFF} are the percentage loads connected with respect to the transformer rating. $P_{EFF.}$ is the effective load connected on the transformer low voltage side and is calculated as a percentage of ratio of $P_{DIFF.}$ to the transformer rating. The negative values of loads in this case implies that the inverter is feeding power to the grid.

From Table II, it can be seen that the peak voltage varies with the effective loading of the transformer and not the actual loading. The deviation of the peak occurring at -0.8 % of transformer rating instead of 0 % is due to the losses in the filter resistor of the inverter.

VI. ANALYSIS OF EFFECT OF ADDITION OF DER

The direction of current flows in the transformer are shown in Figure 11, in which the line parameters have been ignored for simplicity. The effective load connected on the low voltage side of the transformer can be calculated as shown in Equation 5.

In Equation 5, $Z_{EFF.}$ is the effective load impedance connected to the transformer's low voltage side which depends on the voltage on the low voltage side, $\tilde{V}_{LV}$ and the current flowing from the grid to the transformer's low voltage side, $\tilde{I}_{GRID}$. $\tilde{I}_{GRID}$ inturn depends on the current drawn by the load, $\tilde{I}_{LOAD}$ and the current output of the inverter, $\tilde{I}_{INV}$.

$$Z_{EFF.} = \frac{\tilde{V}_{LV}}{\tilde{I}_{GRID}} = \frac{\tilde{V}_{LV}}{\tilde{I}_{LOAD} - \tilde{I}_{INV}} \quad (5)$$

The addition of solar generation in the network can be considered for three different scenarios depending on the total generation from each inverter and the total load connected on each of the transformers. In each of these scenarios, the total generation has been set to the maximum power output of the inverter, which is 7.6 kW.

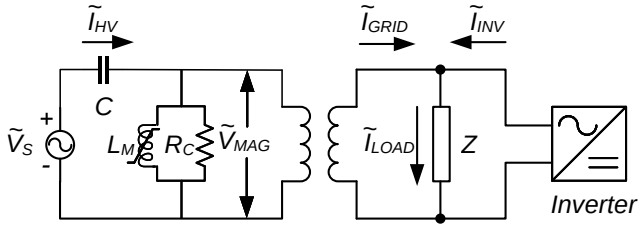

Figure 11 Circuit with series capacitance due to open phase and addition of inverter with line impedances neglected

- **Scenario 1**- $\tilde{I}_{LOAD} > \tilde{I}_{INV}$
  When the load current is more than the inverter output current, the grid current on the transformer low voltage side is the difference of the inverter output current and the load current. In this case, the $Z_{EFF.}$ in Equation 5 increases, thus the transformer presents itself as lightly loaded to the grid.
- **Scenario 2**- $\tilde{I}_{LOAD} \approx \tilde{I}_{INV}$
  When the load and generation are equal, there is no current flow from the grid and $\vec{I}_{GRID} \approx 0$. There is still some reactive current flow due to the filter capacitance and the to feed the inductive part of the load connected.
- **Scenario 3**- $\tilde{I}_{LOAD} < \tilde{I}_{INV}$
  When the load connected is less than the output of the inverter, the inverter feeds current to the grid. The direction of flow of I_{GRID} in this case is thus reversed.

$$\tilde{I}_{GRID} = -(\tilde{I}_{LOAD} - \tilde{I}_{INV}) \quad (6)$$

The capacitor on the source side in Figure 11 represents the capacitance which gets connected in series when the X-phase is opened. $\tilde{I}_{HV}$ is the current flowing through the series capacitor C, $\tilde{V}_S$ is the source voltage and $\tilde{V}_{MAG}$ is the voltage across the magnetizing branch which is also the voltage on the high voltage side of the transformer. ω is the system frequency in radian/second.

According to [34], the voltage across the magnetizing branch can be represented as shown in Equation 7. This equation applies when the direction of flow of current is as shown in the circuit, as described by Scenario 1 previously.

$$\tilde{V}_{MAG} = \tilde{V}_s + \frac{\tilde{I}_{HV}}{\omega c} \quad (7)$$

However, when the inverter current is more than the load current, as described in Scenario 3, the direction of $\tilde{I}_{HV}$ is reversed. The equation can be rewritten as Equation 8. From this equation, it is seen that the voltage across the magnetizing branch is reduced, thus preventing the transformer core from saturating.

$$\tilde{V}_{MAG} = \tilde{V}_s + \frac{(-\tilde{I}_{HV})}{\omega c} \quad (8)$$

It is observed that overvoltages appear in the network when the effective load is positive and its magnitude is very low.

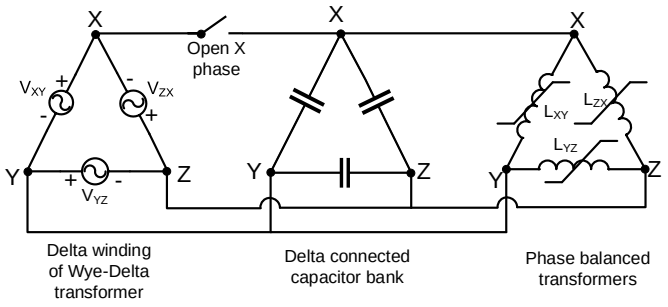

Figure 12. Prevention of ferroresonance by phase balancing

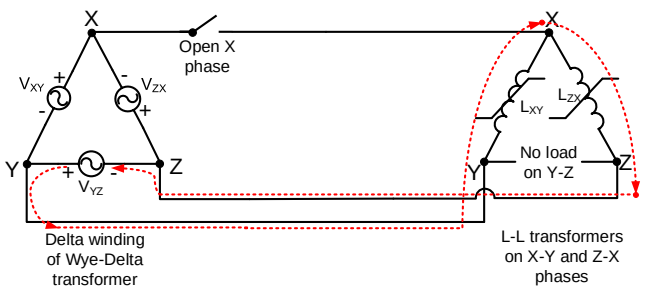

Figure 13. Modified circuit after removal of capacitor bank

Table III
COMPARISON OF VOLTAGES BY ADDING LOADS ON Y-Z PHASE

Number of transformers on Y-Z phase	X-Y peak voltage (p.u.)	Z-X peak voltage (p.u.)
0	2.0985	1.8887
1	0.5025	0.5441
2	0.5001	0.5427
3	0.4978	0.5416
4	0.4961	0.5398

However, it should be noted that the actual load connected in this scenario is more than 35% of the transformer rating, which is usually considered to be sufficient to damp the overvoltages [26] without any generation connected on the transformer low voltage side.

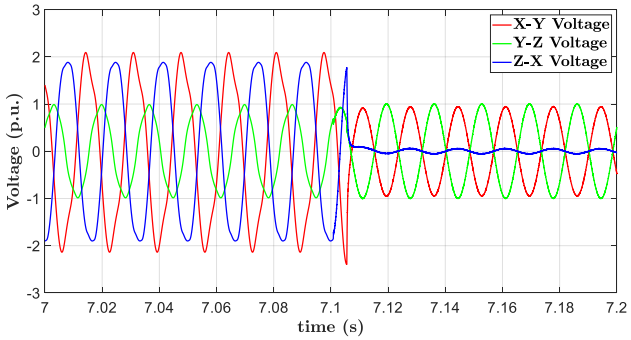

Figure 14. Comparison of voltages before and after switching of capacitor bank

VII. PREVENTION AND MITIGATION

In addition to the prevention and mitigation solutions discussed in Section I, some configuration specific solutions were simulated and will be described in this section. Prevention solution would avoid the initiation of ferroresonance in the circuits similar to the one discussed in this paper. Mitigation solution would stop the sustained overvoltage in the network.

A. Prevention solution

As described in section II, the network has no Y-Z connected transformers, which makes the system unbalanced. Simulations were performed with the loads on the phases balanced. It was observed from the simulations that the addition of even one transformer on the Y-Z phase could have eliminated the occurrence of the overvoltage event. The equivalent circuit with the phase balancing done has been presented in Figure 12. The comparison of peak voltages on the X-Y and Z-X phases after adding transformers on the Y-Z phase is shown in Table III.

On comparing Figure 2 and Figure 12, it can be observed that the addition of the transformer on the Y-Z phase prevents the series connection of the capacitor and the inductor.

B. Mitigation solution

As described in Section II, the shunt capacitor bank in the circuit was controlled based on the time-of-day. By observing the pre-disturbance voltage magnitudes from Figures 3 and 4, it can be seen that the voltage magnitudes were within the permissible limits of 228-252 V (240V±5%) and closer to the higher limit.

Hence, the mitigation solution proposed was to control the capacitor bank based on the voltage measured rather than the time-of-day. Even if the voltage during the steady state would have been close to the lower limit, the overvoltages would have triggered the capacitor bank to be disconnected from the network.

Figure 13 shows the modified circuit and the current path based on Figure 2. The disconnection of the shunt capacitor bank after single-phase operation eliminates the series connection between the capacitor and the transformer core.

Figure 14 shows the comparison between the voltages before and after disconnecting the shunt capacitor bank. The shunt capacitor bank was in service before it was disconnected at 7.1 seconds. After disconnecting the capacitor bank, the voltages dropped to the steady state operating values of 1 p.u. on the X-Y and the Y-Z phases. The voltage on the Z-X phase dropped to almost 0 p.u. due to the X-phase being opened and the strong coupling between the X and Z phases in the cable section.

When disconnecting capacitor banks, high frequency transient overvoltages can occur in the circuit. To verify if any such transient overvoltages were observed in this case, simulations were performed by varying the instant of opening the capacitor bank for points 1 millisecond apart for 1 cycle of the 60 Hz wave. In this study, no such overvoltage was observed. In addition, the capacitor bank controller being used in the network also has a built-in synchronized switching feature.

VIII. CONCLUSIONS

From the simulations performed and comparison of the results with the measurements obtained from the day of the event, it can be concluded that the event was likely caused by ferroresonance. The simulation results are in agreement

with the measurements, but do not match exactly due to the unknowns on the day of the event and the assumptions made.

The prevention of ferroresonance in an unbalanced distribution circuit through the simulations performed proved that a balanced network is less likely to experience a ferroresonance event as opposed to a highly unbalanced network, like the one studied in this paper. Also, based on the mitigation solution explored, it can be seen that the event would not have taken place, had there been no capacitor bank connected on the system. Since the capacitor bank was controlled based on the time-of-day rather than on voltage measurements, one of the recommendations that can be made based on this study is to operate capacitor banks in the system based on the voltage profile. This is important, especially with implementations such as CVR/VVO being increasingly implemented on the distribution systems.

The solar inverters connected on the low voltage side of the distribution transformers can also affect the occurrence of ferroresonance in the distribution systems as proven with an averaged model for the inverters. The averaged model is very efficient to implement and has less computational overhead thereby allowing the simulation of very large systems.

There need to be more studies performed to compare the average models with the switched models, determine the effect of switching harmonics and inverter filter and to implement the response of the inverters in accordance with IEEE-1547 [3] to understand the effects completely.

IX. Acknowledgment

The authors would like to thank National Electric Energy Testing, Research and Applications Center (NEETRAC) for the measurement studies carried out by them on the transformers, which were used for simulation studies.

References

[1] "Necessity of Standardized Procedures for CVR Measurement and Verification," Tech. Rep. IEEE PES- TR91, August 2021.

[2] "IEEE Guide for the Application of Shunt Power Capacitors," *IEEE Std 1036-2010 (Revision of IEEE Std 1036-1992)*, pp. 1–88, 2011.

[3] "IEEE Standard for Interconnection and Interoperability of Distributed Energy Resources with Associated Electric Power Systems Interfaces," *IEEE Std 1547-2018 (Revision of IEEE Std 1547-2003)*, pp. 1–138, 2018.

[4] F. Ding and M. Baggu, "Coordinated Use of Smart Inverters with Legacy Voltage Regulating Devices in Distribution Systems with High Distributed PV Penetration- Increase CVR Energy Savings," *IEEE Transactions on Smart Grid*, pp. 1–10, 2018.

[5] C. J. Mozina, "Impact of Smart Grids and Green Power Generation on Distribution Systems," *IEEE Transactions on Industry Applications*, vol. 49, no. 3, pp. 1079–1090, 2013.

[6] "IEEE Standard Terminology for Power and Distribution Transformers," *IEEE Std C57.12.80-2010 (Revision of IEEE Std C57.12.80-2002)*, pp. 1–60, 2010.

[7] M. Val Escudero, I. Dudurych, and M. Redfem, "Understanding ferroresonance," in *39th International Universities Power Engineering Conference, 2004. UPEC 2004.*, vol. 3, 2004, pp. 1262–1266 vol. 2.

[8] B. A. Mork, "Understanding and Dealing with Ferroresonance," in *42nd Annual Minnesota Power Systems Conference*, 2006.

[9] CIGRE WG C4.307, "Technical Brochure 569- Resonance and Ferroresonance in Power Networks," p. 170, February 2014.

[10] M. A. Masoum and E. F. Fuchs, "Chapter 2 - Harmonic Models of Transformers," in *Power Quality in Power Systems and Electrical Machines*, 2nd ed., Mohammad A.S. Masoum and Ewald F. Fuchs, Ed. Boston: Academic Press, 2015, pp. 105–205.

[11] L. Bohmann, J. McDaniel, and E. Stanek, "Lightning arrester failure and ferroresonance on a distribution system," *IEEE Transactions on Industry Applications*, vol. 29, no. 6, pp. 1189–1195, 1993.

[12] R. H. Miller, "A Study of Ferroresonant Conditions on Distribution Circuits Involving Cable-connected Power Transformers," Master's thesis, South Dakota State University, 1972.

[13] R. Dugan, "Examples of ferroresonance in distribution," in *2003 IEEE Power Engineering Society General Meeting (IEEE Cat. No.03CH37491)*, vol. 2, 2003, pp. 1213–1215 Vol. 2.

[14] A. B. Nassif, M. Dong, S. Kumar, and G. Vanderstar, "Managing Ferroresonance Overvoltages in Distribution Systems," in *2019 IEEE Canadian Conference of Electrical and Computer Engineering (CCECE)*, 2019, pp. 1–4.

[15] P. E. Sutherland and R. Manning, "Ferroresonance in a 13.8kV Distribution Line," in *Conference Record of the 2006 IEEE Industry Applications Conference Forty-First IAS Annual Meeting*, vol. 5, 2006, pp. 2238–2241.

[16] M. Ahmed, A. Ali, S. Mohammed, A. Karrar, R. W. Hay, and R. C. Johnson, "Investigation of Ferroresonance Incidents in the EPB Distribution Network," in *2018 IEEE Power & Energy Society General Meeting (PESGM)*, 2018, pp. 1–5.

[17] S. Hassan, M. Vaziri, and S. Vadhva, "Review of ferroresonance in power distribution grids," in *2011 IEEE International Conference on Information Reuse Integration*, 2011, pp. 444–448.

[18] G. Mokryani, M.-R. Haghifam, H. Latafat, P. Aliparast, and A. Abdollahy, "Analysis of ferroresonance in a 20kV distribution network," in *2009 2nd International Conference on Power Electronics and Intelligent Transportation System (PEITS)*, vol. 1, 2009, pp. 31–35.

[19] Y. Yu and H. Zhou, "Study on Simulation of Ferroresonance Elimination in 10kV Power System," in *2005 IEEE/PES Transmission Distribution Conference & Exposition: Asia and Pacific*, 2005, pp. 1–7.

[20] Y. N. Ryzhkova and S. A. Tsyruk, "Ferroresonance suppression in distribution networks," in *2016 2nd International Conference on Industrial Engineering, Applications and Manufacturing (ICIEAM)*, 2016, pp. 1–4.

[21] W. Wang, X. Shi, A. Huque, and T. Key, "Impact of Interconnection Transformer Configuration on Operation of Inverter-Based DER," in *2021 IEEE 48th Photovoltaic Specialists Conference (PVSC)*, 2021

[22] N. Thanomsat and B. Plangklang, "Ferroresonance phenomenon in PV system at LV side of three phase power transformer using of PSCAD simulation," in *2016 13th International Conference on Electrical Engineering/Electronics, Computer, Telecommunications and Information Technology (ECTI-CON)*, 2016, pp. 1–4.

[23] Hans Kristian Høidalen , László Prikler, and Francisco Peñaloza, "ATPDRAW Version 7.0 for Windows Users' Manual," 2019.

[24] M. Davis, D. Costyk, and A. Narang, "Distributed and Electric Power System Aggregation Model and Field Configuration Equivalency Validation Testing," p. 168, July 2003. [Online]. Available: https://www.nrel.gov/docs/fy03osti/33909.pdf

[25] "XIX-G "SATURA" TO DERIVE $\psi-i$ PEAKVALUE CURVES," in *ATP Rulebook*, 2017.

[26] S. Santoso, R. C. Dugan, T. E. Grebe, and P. Nedwick, "Modeling Ferroresonance Phenomena in an Underground Distribution System," in *International Conference on Power Systems Transients, IPST*, 2001.

[27] Georgia Tech Research Corporation, "DTE Pole Top Transformer Testing, Modeling, and Teardown," *NEETRAC Project: 20-087*, pp. 1–59, 2020.

[28] A. Yazdani and R. Iravani, *Voltage-Sourced Converters in Power Systems: Modeling, Control, and Applications*. Wiley-IEEE Press, 2010.

[29] H. Ding, Z. Wang, L. Fan, and Z. Miao, "Modeling and Control of Grid-following Single-Phase Voltage-Sourced Converter," in *2020 52nd North American Power Symposium (NAPS)*, 2021, pp. 1–6.

[30] CIGRE JWG C4/C6.35/CIRED, "CIGRE TB 727- Modelling of inverter-based generation for power system dynamic studies," May 2018.

[31] M. Aredes, E. H. Watanabe, B. Bonatto, E. A. Mertens Jr., L. F. S. Dias, and S. Nosaki, "Comparative Analysis of Shunt Active Filter Models in the EMTP/ATP and SABER Programs," in *International Conference on Power Systems Transients, IPST*, 2003.

[32] Generac Power Systems, Inc. Generac PWRcell. [Online]. Available: https://www.generac.com/all-products/clean-energy/pwrcell

[33] Brantster, Henrik and Kocewiak, Łukasz and Rygg, Atle and Tedeschi, Elisabetta, "Passive Filter Design and Offshore Wind Turbine Modelling for System Level Harmonic Studies," *Energy Procedia*, vol. 80

[34] A. Greenwood, *Electrical transients in power systems*. Wiley, September 1991.